Publishing Excellence Inspiring Progress
ARISTON PUBLICATIONS
Quantum Advances
ISSN: 3143-0724 www.aristonpubs.com/journal/quantum-advances https://doi.org/10.69626/qa.2026.0086

RESEARCH ARTICLE

Exploring a few nonlinear optical properties of doped GaAs quantum dot driven by noise – confinement ratio interplay

Soumyajit Beltharia[1], Bhaskar Bhakti[2], Manas Ghosh[1*]

ABSTRACT: The study explores the profiles of a few important nonlinear optical (NLO) properties of impurity doped GaAs quantum dot (QD). The NLO properties considered are the nonlinear optical rectification (NOR), the second harmonic generation (SHG) and the third harmonic generation (THG). The enquiry aims to understand how the interplay between Gaussian white noise and the confinement ratio (CFR) can fine-tune the above properties. The said interplay comes out to be delicately dependent on the route of incorporation of noise (additive/multiplicative) to the QD system. The interplay governs both the peak values and peak shifts of the NLO properties in rather complicated manner. Moreover, by prudent adjustment of CFR value and mode of application of noise the NLO properties can often be maximized.

Keywords: Quantum Dot; Impurity; Confinement Ratio; Gaussian White Noise; Nonlinear Optical Properties.

Received: 04 July 2026; Revised: 10 August 2026; Accepted: 30 August 2026; Published Online: 09 September 2026

1. INTRODUCTION

The importance of dopant impurity is enormous in carrying out remarkable changes in the electric, magnetic, transport and optical properties of low-dimensional semiconductor nanostructures (LDSNs). Naturally, LDSNs enjoy ubiquitous applications in several sophisticated quantum devices. Above changes are mainly caused by the delicate interplay between the basic confinement potential of LDSN and the impurity potential [1–26]. Nonlinear optical (NLO) properties emerge as an outcome of the nonlinear response of a material to the strength of the incident optical radiation. Generally, we observe large NLO response if the transition matrix element becomes appreciable. Extensive research on the NLO properties of doped LDSN has immensely contributed towards design and manufacture of many advanced opto-electronic devices. These devices are capable of producing targeted emission and ultra-fine spectra[27, 28]. Therefore, research works on the NLO properties of LDSN have been going unabated [2, 5, 6, 8, 11, 14, 15, 17, 20, 23, 26, 29, 30].

Nonlinear optical rectification (NOR) is a second-order NLO property that produces a static electric field across the nonlinear material. NOR is the manifestation of a quasi DCpolarization or a single wave emission when an intense light beam passes through the NLO medium. NOR plays crucial role in the detection of radiation in the THz region by applying lasers [31]. Therefore, there is no dearth of studies dealing with NOR of LDSN [32–38]. Second harmonic generation (SHG) and the third harmonic generation (THG) are important second-order and third-order NLO properties responsible for generating light waves having frequencies twice and thrice that of the incident radiation, respectively. SHG exhibits

[1] Department of Chemistry, Physical Chemistry Section, Visva-Bharati University, Santiniketan, Birbhum-731235, West Bengal, India.

[2] Department of Chemical Sciences, Biswa Bangla Biswabidyalay, Birbhum 731204, West Bengal, India.

[*] Author to whom correspondence should be addressed: pcmg77@gmail.com (M. Ghosh)

© Ariston Publications 2026. All rights reserved.

extreme sensitivity to the symmetry of the system. This makes SHG an important probe for examining the second-order properties of surface and interfaces [68] producing considerable amount of research on this property [38–43]. Similarly, THG displays rigorous usage in alloptical switching, modulating and computing devices [44]. Naturally, substantial research activities on THG of LDSNs have also been envisaged [35, 43, 45–52]. The physical properties of LDSN strongly depends on its confinement potential and it has been possible to modulate the confinement potential experimentally [53]. The said modulation can be carried out by means of impurity, external parameters like electric field, magnetic field, temperature, pressure etc and noise. Such modulations invariably help tailor the NLO properties of LDSN.

Current work deals with *GaAs* QD comprising of a lone electron with a constrained motion over the $x-y$ plane subject to a lateral parabolic confinement potential. The QD confinement potential also involves a magnetic field perpendicular to the $x-y$ plane. The QD incorporates Gaussian impurity as dopant and Gaussian white noise has been applied via additive and multiplicative routes. In practice, lateral confinement is often exploited to produce QDs since such confinement arrests the motion of the electrons which were originally locked in an extremely narrow quantum well. The transverse dimensions of QDs manufactured in this way overwhelm its thickness making QDs assume a flat disk shape. As an outcome, the excitation energy of the electron across the disk outweighs other relevant energies. The confined electron, thus, becomes virtually two-dimensional [54].

In the present work, the quantities ω_0 and ω_c are the two parameters that represent the inherent confinement frequency for both x and y directions and only for y direction, respectively. ω_c, in effect, comes out to be proportional to the strength of the perpendicular magnetic field. The study strives to explore the resultant effect of these two confinement frequencies (tantamount to confinement potentials) on NOR, SHG and THG of doped *GaAs* QD in presence of Gaussian white noise. In view of this the *confinement ratio (CFR)* is defined as $\omega_r = \omega_c/\omega_0$. The study scrutinizes the profiles of above properties as a function of CFR with and without noise. The scrutiny unveils how the resultant influence of the confinements in the two directions interplays with noise (including the path of application of noise) and governs the above NLO properties.

2. METHOD

The QD Hamiltonian containing impurity and under applied Gaussian white noise reads

$$H_0 = H_0' + V_{imp} + \xi(x,y). \tag{1}$$

H_0' represents the QD Hamiltonian without dopant, which, under effective mass approximation, can be written as

$$H_0' = \frac{1}{2m^*}\left[-i\hbar\nabla + \frac{e}{c}\mathbf{A}\right]^2 + \frac{1}{2}m^*\omega_0^2(x^2+y^2). \tag{2}$$

H_0' contains the lateral parabolic confinement $\frac{1}{2}m^*\omega_0^2(x^2+y^2)$, where, ω_0 and m^* represent the confinement frequency and the electronic effective mass, respectively. The vector potential $\mathbf{A}$, in Landau gauge, can be defined as $[A=(By,0,0)]$, where B is the magnetic field strength. More explicitly, H_0' can be written as [55, 56]

$$H_0' = -\frac{\hbar^2}{2m^*}\left(\frac{\partial^2}{\partial x^2}+\frac{\partial^2}{\partial y^2}\right) + \frac{1}{2}m^*\omega_0^2x^2 + \frac{1}{2}m^*\Omega^2y^2 - i\hbar\omega_c y\frac{\partial}{\partial x} \tag{3}$$

where the cyclotron frequency (ω_c) is given by

$$\omega_c\left(=\frac{eB}{m^*c}\right) \text{ and } \Omega = \sqrt{\omega_0^2+\omega_c^2}.$$

Thus, whereas the confinement frequency ω_0 becomes present in both x and y directions, the other confinement frequency, viz. ω_c becomes present only in y direction and is simply proportional to B. We now define the *confinement ratio (CFR)* as $\omega_r = \omega_c/\omega_0$.

The impurity potential V_{imp} of eqn(1) has been chosen to be Gaussian [57, 58]. It can be written as

$$V_{imp} = V_0\, e^{-\gamma[(x-x_0)^2+(y-y_0)^2]}. \tag{4}$$

Above impurity potential is endowed with three typical impurity parameters, viz. (x_0,y_0), V_0 and γ, where (x_0,y_0) and V_0 represent the dopant coordinate and the dopant potential strength, respectively. And $\gamma^{-1/2}$ gives us an impression of the spatial stretch over which the impurity potential remains meaningful.

Mathematically, applied Gaussian white noise is represented by the function $\xi(x,y)$ of eqn(1). A second function $g(x,y)$ is now needed which ensures the two main features of such noise viz. *zero-mean* and *spatial* δ*-correlation*. Moreover, based on the mode of linkage between $\xi(x,y)$ and $g(x,y)$, noise being additively or multiplicatively introduced to the QD system. $g(x,y)$ satisfies the following two conditions standing for zero mean and spatial δ-correlation, respectively:

© Ariston Publications 2026. All rights reserved.

$$\langle g(x,y)\rangle = 0 \tag{5}$$

and

$$\langle g(x,y)g(x',y')\rangle = 2\zeta\delta\left[(x,y)-(x',y')\right], \tag{6}$$

where ζ is the noise strength. The function $g(x,y)$, satisfying above two conditions while maintaining a Gaussian distribution can be produced by means of Box-Muller algorithm. The final noise function, i.e. $\xi(x,y)$ is linked with $g(x,y)$ in two different ways giving rise to *additive* white noise (WN1) and *multiplicative* white noise (WN2) as outlined below:

$$\xi(x,y) = \lambda_1 g(x,y), \quad \text{for WN1} \tag{7}$$

and

$$\xi(x,y) = \lambda_2 g(x,y)(x+y), \quad \text{for WN2.} \tag{8}$$

λ_1 and λ_2 are the two constants.

Linear variational principle, with the trial function $\psi_k(x,y)$, has been employed for solving the time-independent Schrödinger equation. $\psi_k(x,y)$ is composed of the product of harmonic oscillator eigenstates. Therefore,

$$\psi_k(x,y) = \sum_{nm} c_{nm,k}\,\phi_n(px)\phi_m(qy), \tag{9}$$

$c_{nm,k}$ are the coefficients, $p = \sqrt{\frac{m^*\omega_0}{\hbar}}$ and $q = \sqrt{\frac{m^*\Omega}{\hbar}}$.

This is followed by the construction of the Hamiltonian matrix for H_0 and its subsequent diagonalization to obtain the normalized eigenvectors and the energy eigenvalues.

Now, determination of the NLO properties requires consideration of a polarized monochromatic electromagnetic field of angular frequency ν incident on an ensemble of QDs. This is followed by density matrix treatment and iterative procedure which ultimately give the analytical expressions of NOR, SHG and THG for optical transitions between the ground and the excited states.

2.1 Nonlinear Optical Rectification (NOR)

The NOR coefficient under two-level system approximation can be given by [35]

$$\chi_0^{(2)} = \frac{4e^3\sigma_s}{\varepsilon_0\hbar^2}M_{ij}^2\delta_{ij} \times \frac{\Delta E_{ij}^2\left(1+\Gamma_2/\Gamma_1\right)+\left(\nu^2+\Gamma_2^2\right)\left(\Gamma_2/\Gamma_1-1\right)}{\left[\left(\Delta E_{ij}-\nu\right)^2+\Gamma_2^2\right]\left[\left(\Delta E_{ij}+\nu\right)^2+\Gamma_2^2\right]} \tag{10}$$

where e, σ_s, ε_0 and ν are the absolute value of electron charge, the carrier density, the permittivity of vacuum and the transition frequency, respectively.

$M_{ij} = e\langle\psi_i|\hat{x}+\hat{y}|\psi_j\rangle, (i,j=1,2)$ are the dipole matrix elements. $\delta_{ij} = |M_{ii}-M_{jj}|$. $\psi_i(\psi_j)$ and $\Delta E_{ij} = (E_i-E_j)/\hbar$ are the eigenstates and the energy interval between these states, respectively. $\Gamma_k = 1/T_k$ with $k = (1,2)$ are damping terms associated with the lifetime (longitudinal and transverse, respectively) of the electron being excited.

For $\nu \approx \Delta E_{12}$, we can write the expression of NOR peak value as [33]

$$\chi_{0,max}^{(2)} = 2e^3T_1T_2\sigma_s M_{12}^2\delta_{12}/(\varepsilon_0\hbar^2). \tag{11}$$

2.2 Second Harmonic Generation (SHG)

Under two-photon resonance condition (i.e. $\hbar\nu = \hbar\nu_{21} = \hbar\nu_{32}$) and for a three-level quantum system, the SHG susceptibility per unit volume can be expressed as [41]

$$\chi_{2\nu}^{(2)} = \frac{e^3\sigma_s}{\varepsilon_0\hbar^2}\frac{|M_{12}|.|M_{23}|.|M_{31}|}{\left(\nu-\nu_{21}+i\Gamma_{21}\right).\left(2\nu-\nu_{31}+i\Gamma_{31}\right)}, \tag{12}$$

$\Gamma = \Gamma_{21} = \Gamma_{31}$ is the off-diagonal relaxation rate.

The SHG susceptibility reveals a maximum relevant to two-photon resonance ($\hbar\nu = \hbar\nu_{21} = \hbar\nu_{32} = \hbar\nu_{31}/2$) given as [38]

$$\chi_{2\nu,max}^{(2)} = \frac{e^3\sigma_s}{\varepsilon_0}\frac{|M_{12}|.|M_{23}|.|M_{31}|}{(\hbar\Gamma)^2}. \tag{13}$$

The SHG peak value becomes proportional to the geometric factor (GF) $|M_{12}|.|M_{23}|.|M_{31}|$. Therefore, monitoring the GF would evidently explain the variation of SHG peak value with change in physical quantities. For a quantum system having

© Ariston Publications 2026. All rights reserved.

inversion symmetry the wave functions are either symmetric or asymmetric, the dipole matrix element $|M_{31}|$ disappears and hence the SHG [40].

2.3 Third Harmonic Generation (THG)

Triple resonance condition gives the expression of THG susceptibility per unit volume [47]

$$\chi_{3\nu}^{(3)} = \frac{e^4\sigma_s}{\varepsilon_0\hbar^3}\frac{M_{12}\cdot M_{23}\cdot M_{34}\cdot M_{41}}{(\nu-\nu_{21}+i\Gamma_{21})} \times \frac{1}{(2\nu-\nu_{31}+i\Gamma_{31})\,(3\nu-\nu_{41}+i\Gamma_{41})} \tag{14}$$

$\Gamma_{ij}(i\neq j)=\Gamma_2=1/T_2$ being the off-diagonal relaxation rate and T_2 is the transverse relaxation time.

Under triple resonance condition the THG resonant peak appears at energy corresponding to $\hbar\nu=\hbar\nu_{21}=\hbar\nu_{32}=\hbar\nu_{43}=\hbar\nu_{41}/3$ and reads [47]

$$\chi_{3\nu,max}^{(3)} = \frac{e^4\sigma_s}{\varepsilon_0}\frac{|M_{12}|.|M_{23}|.|M_{34}|.|M_{41}|}{i\,(\hbar\Gamma_2)^3}, \tag{15}$$

where the off-diagonal relaxation rate $\Gamma_2=\Gamma_{21}=\Gamma_{31}=\Gamma_{41}$. The geometric factor $(|M_{12}|.|M_{23}|.|M_{34}|.|M_{41}|)$ gives the THG peak value $(\chi_{3\nu,max}^{(3)})$ under resonance condition [47].

3. RESULT AND DISCUSSION

In general, the values of various physical parameters used in the present study are as follows: $m^*=0.067m_0$, where m_0 is the free-electron mass, $\varepsilon_0=8.8542\times10^{-12}Fm^{-1}$, $\sigma_s=5.0\times10^{24}m^{-3}$, $\tau=0.14$ ps, $\hbar\omega_0=100.0$ meV, $B=5.0$ T, $V_0=-200.0$ meV, $(x_0,y_0)=(0,0)$ (on-center dopant) and $\zeta=1.0\times10^{-4}$, respectively. These values are spread out in various papers and do not require any specific citations.

In the forthcoming discussions it would be found that the features of various NLO properties noticeably depend on the mode of application of noise (WN1 or WN2). Thus, prior to the said discussion, we elucidate the importance of noise mode to avoid repetition and keep the manuscript brief. The dependence of the features of the NLO properties on noise mode stems from the fact that WN1 and WN2 modify the QD confinement in diverse ways. Whereas WN2 makes a rather strong coupling with the noise-free system, the coupling becomes relatively weak in case of WN1. As a result, the effective confinement of the system becomes different under WN1 and WN2 resulting into emergence of diverse features in the NLO properties. A varying CFR, along with noise (including its mode) actually govern the overlap between the relevant eigenstates and the energy level separations. Thus, the magnitude of the NLO properties is also affected. The complex interplay between the CFR and the noise mode influences the overlap between the eigenstates and the energy intervals in such a subtle way that the profiles of the NLO properties often become non-monotonic. In consequence, we observe maximization/minimization in the NLO profiles.

3.1 Nonlinear optical rectification (NOR)

Figure 1a-c depict the NOR diagrams as a function of the incoming photon energy for five different values of CFR, in absence of noise and under WN1 and WN2, respectively. In absence of noise and under applied WN1 the NOR peaks reveal monotonic red-shift as CFR increases. On the other hand, in presence of WN2, the NOR peaks do not reveal any observable shift as the CFR changes. Earlier we have mentioned that a steady increase in CFR brings about some kind of contrasting changes in the confinement. It causes simultaneous growth of y-confinement as well as a fall of both x and y confinements. The nature of the peak shift indicates that, without noise and under WN1, there occurs a net reduction in the QD confinement as CFR increases. This leads to the fall of the energy level separations giving rise to the red-shifts [36]. However, in presence of WN2, the overall confinement attains some sort of saturation with respect to CFR thereby denying any peak shift.

Figure 1d delineates the variation of NOR peak height against CFR in presence and absence of noise. Under noise-free state and in presence of WN2 the NOR peak values show minimization in the vicinity of $\omega_r\sim1.0$. Under applied WN1, the peak height exhibits a steady growth with increase in CFR. The enhancement of NOR is said to be related with increase in asymmetry of the system [35] and thus to the enhancement of the geometric factor (GF), viz. $M_{12}^2\delta_{12}$ [33]. The magnitude of NOR coefficient depends on the square of the dipole matrix elements and also on the energy interval in a complex way. In general, a reduction of confinement potential causes an increment of the extended areas of the wave functions. In consequence, the extent of overlap between the wave functions increases, which,

© Ariston Publications 2026. All rights reserved.

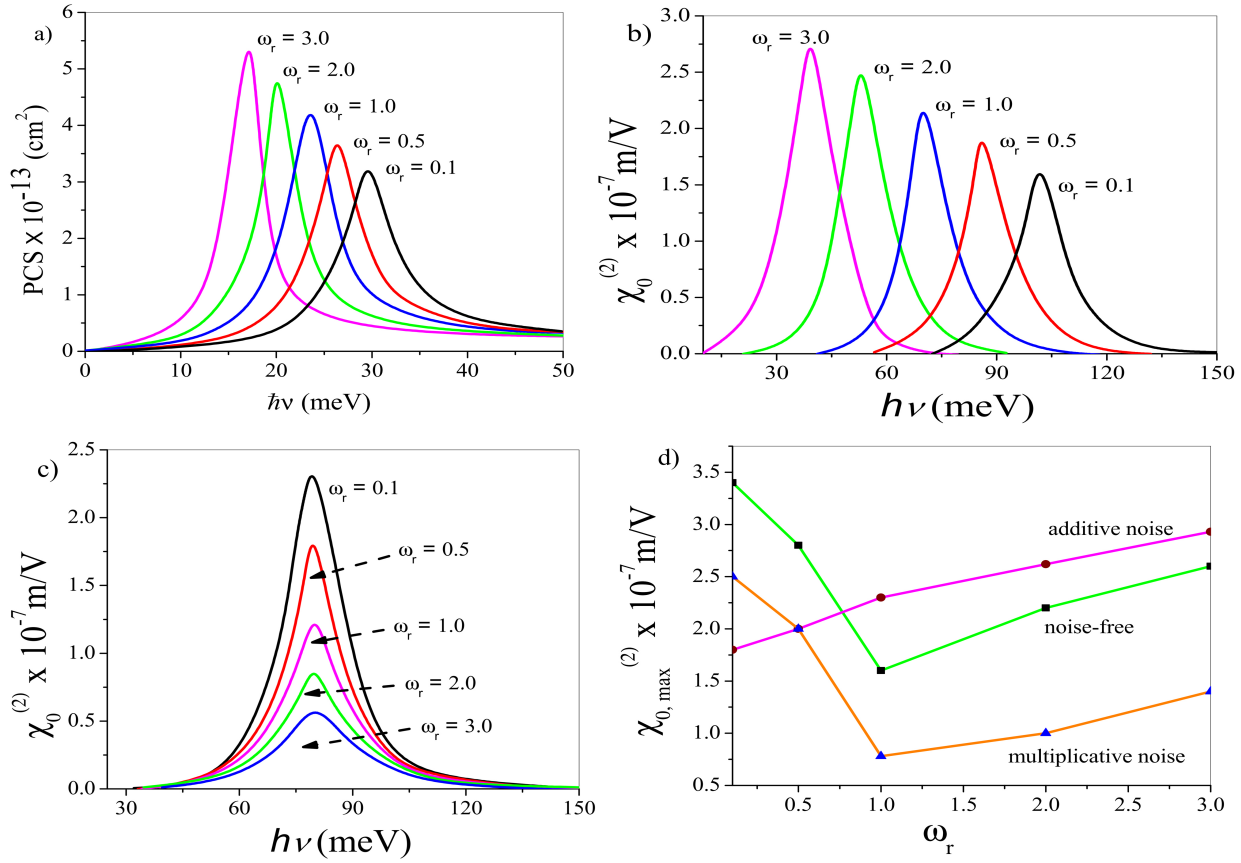


Fig. 1. Plots of NOR vs $h\nu$ for five different values of CFR: (i) $\omega_r = 0.1$, (ii) $\omega_r = 0.5$, (iii) $\omega_r = 1.0$, (iv) $\omega_r = 2.0$ and (v) $\omega_r = 3.0$: (a) devoid of noise, (b) with WN1 and (c) with WN2. (d) Plots of NOR peak heights vs CFR: (i) without noise, (ii) under WN1 and (iii) under WN2.

in turn, raises the magnitude of the dipole moment matrix elements. Thus, a fall of confinement usually increases the NOR peak intensity [36]. Conversely, an increase in the confinement makes the electron more energy rich leading to a diminish in the overlap between the concerned eigenstates. As a result, the NOR peak height decreases [36, 37]. In all situations the overall variation of NOR peak intensity with CFR depends sensitively on the energy intervals and the dipole matrix elements [26]. Presence of noise (including its mode of application) makes the scenario much more complicated. However, in case of NOR, superseding the other parameters, the peak values are principally guided by the asymmetric character of the system. The findings suggest that, without noise and in presence of WN2, as a result of complex interplay mentioned above, the asymmetric nature of the system minimizes around $\omega_r \sim 1.0$, whereas, under WN1, the said interplay steadily augments the asymmetric nature of the system with increase in CFR.

3.2 Second harmonic generation (SHG)

Figure 2a-c describe the SHG profiles against the changing incident photon energy for five different values of CFR, both with and without noise. In absence of noise and under applied WN1 the SHG peaks evince steady red-shift as CFR increases. On the other hand, in presence of WN2, the SHG peaks remain unshifted with the change of CFR. It has been previously mentioned that a monotonic enhancement of CFR causes kind of contrasting changes in the confinement. It causes enhancement of the y-confinement and diminish of both x and y confinements at the same time. The pattern of the peak shift indicates that, without noise and under WN1, there occurs an overall depletion of the QD confinement as CFR enhances. The said depletion reduces the energy intervals giving rise to the red-shifts [38, 42]. However, in presence of WN2, the overall confinement culminates in saturation with increase in CFR and the SHG peaks remain unshifted.

© Ariston Publications 2026. All rights reserved.

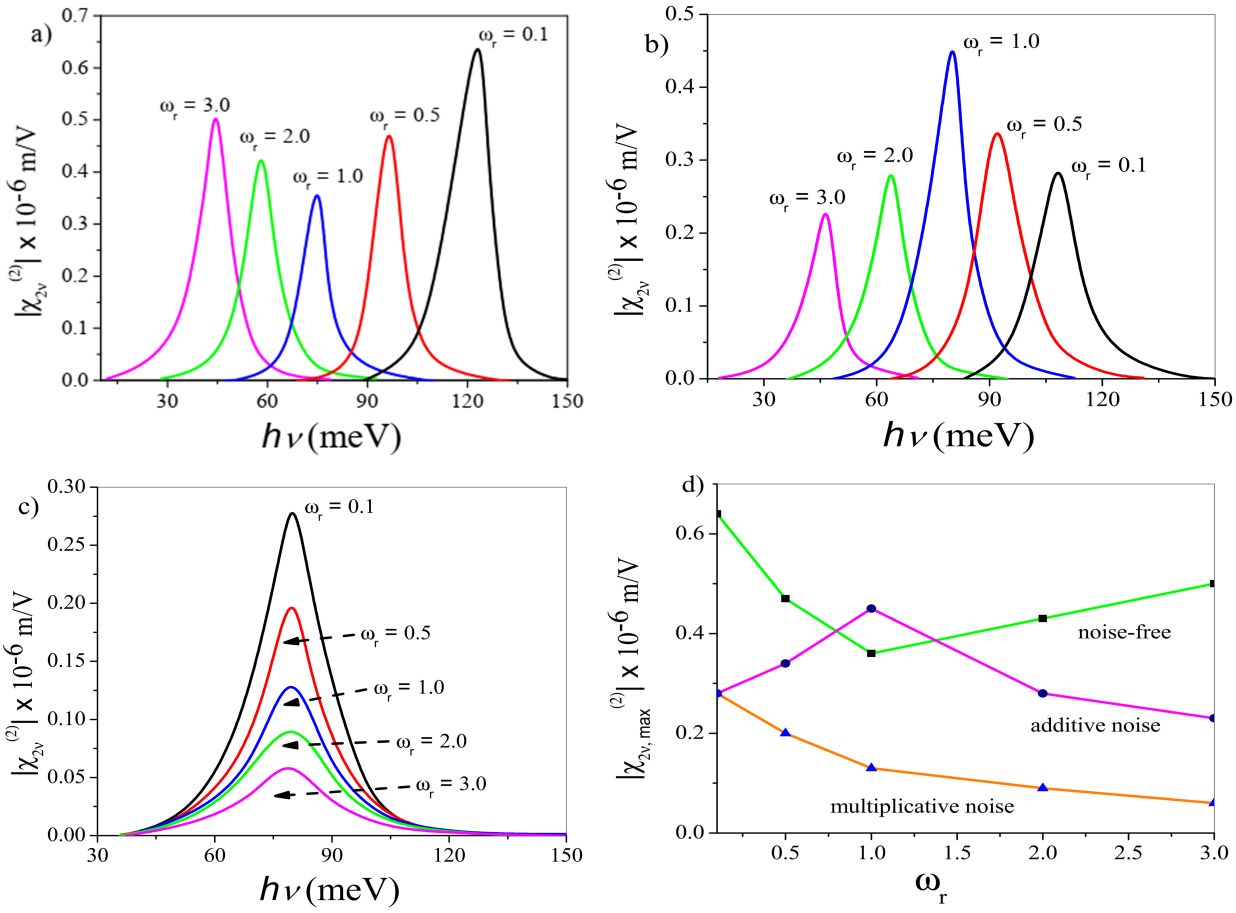


Fig. 2. Profiles of SHG vs $h\nu$ for five different values of CFR: (i) $\omega_r = 0.1$, (ii) $\omega_r = 0.5$, (iii) $\omega_r = 1.0$, (iv) $\omega_r = 2.0$ and (v) $\omega_r = 3.0$: (a) devoid of noise, (b) with WN1 and (c) with WN2. (d) Plots of SHG peak heights vs CFR: (i) without noise, (ii) under WN1 and (iii) under WN2.

Figure 2d delineates the variation of SHG peak height against CFR in presence and absence of noise. In absence of noise and under WN1 the SHG peaks undergo minimization and maximization, respectively, in the vicinity of $\omega_r \sim 1.0$. Under applied WN2, on the other hand, the SHG peaks manifest steady decline with increase in CFR. Generally, a decrease in system confinement makes the wave function spread over a wider region (the extended areas of wave function) thereby enhancing its scope of overlap [41]. However, in case of SHG, apart from the asymmetry factor the energy level separations also play an even more dominant role. Thus, the pattern of variation of SHG peak heights with CFR appears to be different from that in case of NOR. Therefore, in case of SHG, the dominant role of energy intervals, coupled with the somewhat weaker role of wave function overlap and applied noise (including its pathway of application) determine the overall pattern of variation of SHG plots against CFR.

3.3 Third harmonic generation (THG)

Figure 3a-c manifest the THG profiles against the impinging photon energy for five different values of CFR, both considering and ignoring noise. Under noise-free state and in presence of WN1 the THG peaks exhibit steady red-shift as CFR increases [46, 48, 50–52]. On the other hand, under applied WN2, the THG peaks do not undergo any shift as CFR increases. The observation reflects that, without noise and under WN1, the QD confinement suffers an overall depletion with increase in CFR. The depletion enhances the effective parabolic well width [45] and reduces the energy intervals resulting into the red-shift. Under applied WN2, on the other hand, the overall confinement settles to some steady value as CFR increases and the THG peaks remain unshifted.

© Ariston Publications 2026. All rights reserved.

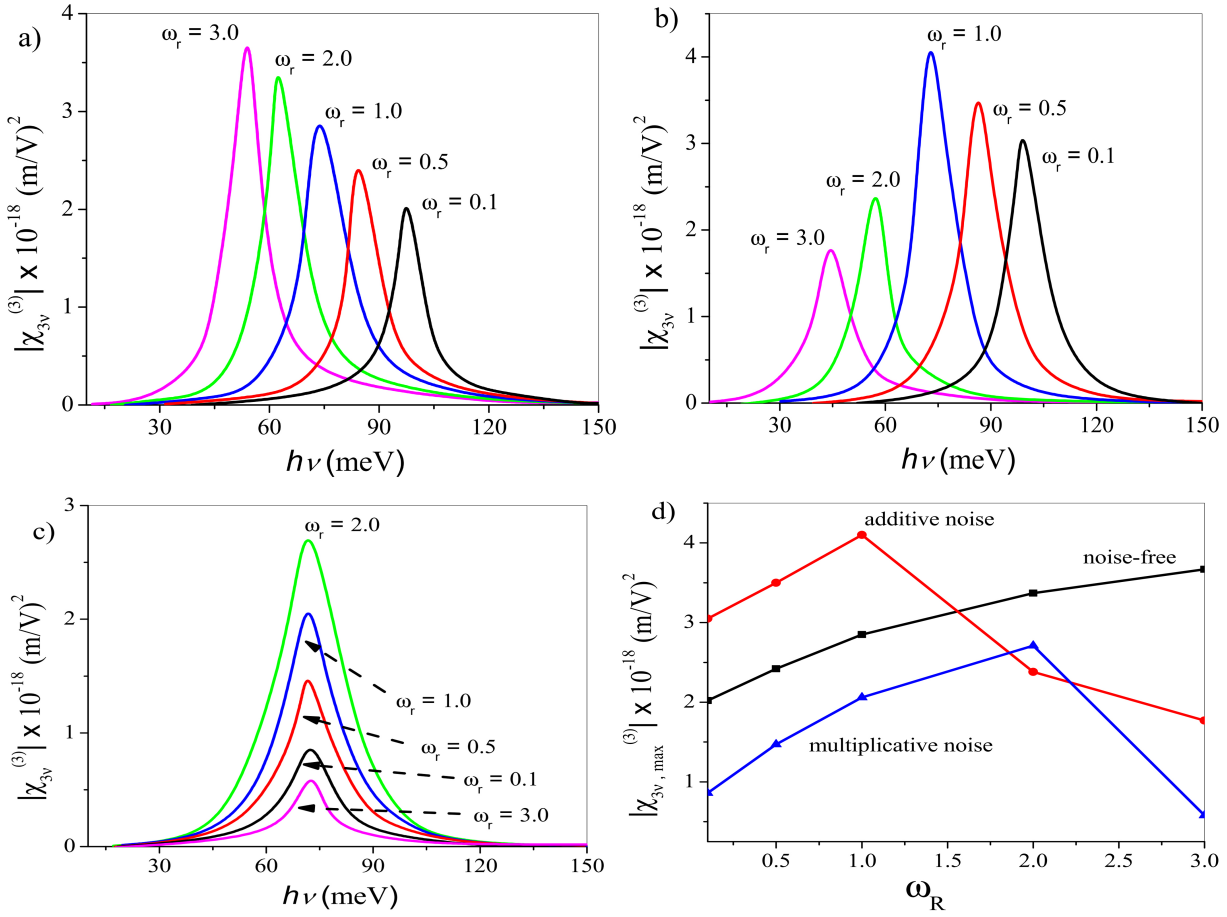


Fig. 3. The THG curves vs $h\nu$ for five different values of CFR: (i) $\omega_r = 0.1$, (ii) $\omega_r = 0.5$, (iii) $\omega_r = 1.0$, (iv) $\omega_r = 2.0$ and (v) $\omega_r = 3.0$: (a) free of noise, (b) considering WN1 and (c) considering WN2. (d) Plots of THG peak heights vs CFR: (i) noise-free state, (ii) under WN1 and (iii) under WN2.

4. CONCLUSION

The influence of subtle interplay between the confinement ratio (CFR) and noise on a few NLO properties (NOR, SHG and THG) of impurity doped *GaAs* QD has been minutely examined. The said interplay reveals noticeable dependence on the pathway of application (additive/multiplicative) of noise.

All the NLO properties evince prominent red-shift of their peaks in absence of noise and under applied WN1 with increase in CFR. However, under applied WN2, the said peaks remain nearly unshifted as the CFR changes.

From a technological viewpoint emergence of large NLO properties is quite desirable. In view of this, one has to keep the CFR away from unity to get large NOR coefficient in absence of noise and under WN2. However, under applied WN1, a large value of CFR appears to be conducive for the production of large NOR.

For the production of large SHG under noise-free state one needs to keep CFR away from unity. However, in presence of WN1, maximum SHG can be obtained in the vicinity of CFR $\sim$ 1.0. And in presence of WN2, large SHG can be expected for very low values of CFR.

In absence of noise, high value of CFR is required for generation of large THG. However, emergence of THG can be maximized in presence of noise by keeping CFR in the vicinity of 1.0 for WN1 and 2.0 for WN2, respectively.

DECLARATIONS

Acknowledgements

The authors S. B., B. B. and M. G. thank DST-FIST (Government of India) and UGCSAP (Government of India) for support

© Ariston Publications 2026. All rights reserved.

Ethical Approval

We affirm that this manuscript is an original work, has not been previously published, and is not currently under consideration for publication in any other journal or conference proceedings. All authors have reviewed and approved the manuscript, and the order of authorship has been mutually agreed upon.

Funding

Funding not available

Availability of data and material

The datasets used and/or analyzed during the current study are available from the corresponding author on reasonable request.

Author's contributions

All the authors contributed substantially to the paper.

Conflicts of Interest

The authors declare that they have no financial or personal interests that could have influenced the research and findings presented in this paper. The authors alone are responsible for the content and writing of this article.

Data Availability

This manuscript has no associated data added to any data repository.

REFERENCES

[1] Tshipa, M. Nkoni, G. K., **2020**. Donor Binding Energies in a Spherical Core-Shell Quantum Dot:. *Indian Journal of Physics*, 94, p.633-638. https://doi.org/10.1007/s12648-019-01513-8.

[2] Bahar, M. K. Başer, P., **2023**. Combined Effects of Thermodynamic Factors External Fields for Nonlinear. *Physics Letters A*, 483, p.129046. https://doi.org/10.1016/j.physleta.2023.129046.

[3] Yakar, Y. Çakır, B. Özmen, A., **2025**. Analysis of Electronic Structure Binding Energy in Five-. *Advanced Theory Simulations*, 8, p.2401375. https://doi.org/10.1002/adts.202401375.

[4] Doba, P. Melono, R. L. M. Etindele, A. J. Motapon, O., **2021**. Oscillator Strengths, Transition Probabilities State Lifetimes of On- Off-Center Donor Impurities. *The European Physical Journal D*, 75, p.110. https://doi.org/10.1140/epjd/s10053-021-00130-7.

[5] Restrepo, R. L. Morales, A. L. Martínez-Orozco, J. C. Baghramyan, H. M. Barseghyan, M. G. Mora-Ramos, M. E. Duque, C. A., **2014**. Impurity-Related Nonlinear Optical Properties in Delta-Doped Quantum Rings:. *Physica B: Condensed Matter*, 453, p.140-145. https://doi.org/10.1016/j.physb.2014.05.004.

[6] Zeng, Z. et .al, **2013**. Linear Nonlinear Optical Properties of ZnO/ZnS ZnS/ZnO Core Shell Quantum Dots:. *Journal of Applied Physics*, 114, p.023510. https://doi.org/10.1063/1.4813094.

[7] Belamkadem, L. Mommadi, O. Boussetta, R. Chouef, S. Chnafi, M. El Moussaouy, A. Vinasco,, **2022**. The Intensity Direction of the Electric Field Effects on Off-Center Shallow-Donor Impurity Binding Energy. *Thin Solid Films*, 757, p.139396. https://doi.org/10.1016/j.tsf.2022.139396.

[8] Toscano-Negrette, R. G. León-González, J. C. Vinasco, J. A. Morales, A. L. Koc, F. Kavruk, A. E. Sahin, M. Mora-Ramos, M. E., **2023**. Optical Properties in a ZnS/CdS/ZnS Core/Shell/Shell Spherical Quantum Dot: Electric Magnetic. *Nanomaterials*, 13(3), p.550. https://doi.org/10.3390/nano13030550.

[9] Ed-Dahmouny, A. El-Bakkari, K. Jaouane, M. Hahn, R. V. H. Arraoui, R. Fakkahi, A. Azmi,, **2024**. Electron-Donor-Impurity Polarizability in a Semiconductor Nanostructure under Electric Field. *Physics Letters A*, 509, p.129502. https://doi.org/10.1016/j.physleta.2024.129502.

[10] Pérez, L. M. Aghoutane, N. Laroze, D. Díaz, P. El-Yadri, M. Feddi, E. M., **2023**. Unveiling the Role of Donor Impurity Position on the Electronic Properties in Strained Type I Type II Core/Shell. *Materials*, 16(19), p.6535. https://doi.org/10.3390/ma16196535.

[11] Chouef, S. Mommadi, O. Boussetta, R. Hbibi, M. El Moussaouy, A. Şahin, M. Falyouni, F. Duque, C. A., **2024**. Effects of Surface Curvature Electric Field on Electronic Optical Properties of an Off-Center Hydrogenic Donor. *The European Physical Journal Plus*, 139, p.381. https://doi.org/10.1140/epjp/s13360-024-05164-5.

 © Ariston Publications 2026. All rights reserved.

[12] Eksi, D. Mese, A. I. Cicek, E. Ozkapi, S. G. Ozkapi, B. Erdogan, I., **2025**. Laser Field Effect on Binding Energy Self-Polarization of an Impurity in a Double Square Quantum Well. *Indian Journal of Physics*, 99, p.2269-2278. https://doi.org/10.1007/s12648-024-03449-0.

[13] Mese, A. I. Cicek, E. Ozkapi, S. G. Ozkapi, B. Erdogan, I., **2023**. Calculation of Intradonor Normalized Transition Energy in Spherical Quantum Dots Made of Different Materials. *Physica Status Solidi B*, 260, p.2300133. https://doi.org/10.1002/pssb.202300133.

[14] Haghighatzadeh, A. Tuzemen, A. T. Demir, M. Peter, A. J. Ungan, F., **2025**. Numerical Study of Binding Energies Optical Responses of a Symmetric Modulation-Doped Single Quantum Well. *Applied Physics A*, 131, p.751. https://doi.org/10.1007/s00339-025-08879-z.

[15] Haghighatzadeh, A. Attarzadeh, A. Durmuslar, A. S. Al, E. B. Ungan, F., **2024**. Modeling of Electronic Spectra Optical Responses of a Semiconductor AlGaAs/GaAs Quantum Well with Three-Step Barriers. *The European Physical Journal Plus*, 139, p.353. https://doi.org/10.1140/epjp/s13360-024-05165-4.

[16] Alauwaji, R. M. Dakhlaoui, H. Belhadj, W. Algraphy, E. Al-Shameri, N. S. Ungan, F. Wang, S., **2026**. Characteristics of Harmonic Anharmonic Spherical Quantum Dots Modulated by Structural. *Indian Journal of Physics*, 100(2), p.451-461. https://doi.org/10.1007/s12648-025-03781-z.

[17] Yücel, M. B. Sakiroglu, S. Sari, H. Duque, C. A. Kasapoglu, E., **2022**. Influence of External Fields on the Exciton Binding Energy Interb Absorption in a Double Inverse Parabolic Quantum Well. *Physica E: Low-Dimensional Systems Nanostructures*, 144, p.115433. https://doi.org/10.1016/j.physe.2022.115433.

[18] Rastegar Sedehi, H. R. Khordad, R. Bahramiyan, H., **2021**. Optical Properties Diamagnetic Susceptibility of a Hexagonal Quantum Dot: Impurity Effect. *Optical Quantum Electronics*, 53, p.264. https://doi.org/10.1007/s11082-021-02927-7.

[19] Rahmani, M. Servatkhah, M. Setoodeh, V., **2024**. Optical Properties of T-Shaped Quantum Wires Considering Impurity, Temperature Pressure. *Optical Quantum Electronics*, 56, p.1845. https://doi.org/10.1007/s11082-023-05523-z.

[20] Bahramiyan, H. Servatkhah, M., **2015**. Second Third Harmonic Generation of a Hexagonal Pyramid Quantum Dot: Impurity Position Effect. *Optical Quantum Electronics*, 47(8), p.2747-2758. https://doi.org/10.1007/s11082-015-0176-4.

[21] Yaseen, A. Shaer, A. ElSaid, M. K., **2019**. The Magnetic Properties of GaAs Parabolic Quantum Dot in the Presence of Donor. *Chinese Journal of Physics*, 60, p.598-611. https://doi.org/10.1016/j.cjph.2019.05.031.

[22] Elsaid, M. Ali, M. Shaer, A., **2019**. The Magnetization Magnetic Susceptibility of GaAs Gaussian Quantum Dot with Donor Impurity in a Magnetic Field. *Modern Physics Letters B*, 33(34), p.1950422. https://doi.org/10.1142/S0217984919504220.

[23] Mantashian, G. A. Zaqaryan, N. A. Mantashyan, P. A. Sarkisyan, H. A. Baskoutas, S. Hayrapetyan, D. B., **2021**. Linear Nonlinear Optical Absorption of CdSe/CdS Core/Shell Quantum Dots in the Presence of Donor Impurity. *Atoms*, 9(4), p.75. https://doi.org/10.3390/atoms9040075.

[24] Kirak, M. Yilmaz, S., **2022**. Third Harmonic Generation of Spherical Multilayered Quantum Dot: Effects of Quantum Confinement, Impurity. *Applied Physics A*, 128, p.459. https://doi.org/10.1007/s00339-022-05601-1.

[25] Vaseghi, B. Rezaei, G. Sajadi, T., **2015**. Optical Properties of Parabolic Quantum Dots with Dressed Impurity: Combined Effects of Pressure. *Physica B: Condensed Matter*, 456, p.171-175. https://doi.org/10.1016/j.physb.2014.08.034.

[26] Karimi, M. J. Rezaei, G. Nazari, M., **2014**. Linear Nonlinear Optical Properties of Multilayered Spherical Quantum Dots: Effects of Geometrical Size. *Journal of Luminescence*, 145, p.55-60. https://doi.org/10.1016/j.jlumin.2013.07.046.

[27] Schmitt-Rink, S. Chemla, D. S. Miller, D. A. B., **1989**. Linear Nonlinear Optical Properties of Semiconductor Quantum Wells. *Advances in Physics*, 38(2), p.89-188. https://doi.org/10.1080/00018738900101102.

[28] Grillot, F. Duan, J. Dong, B. Huang, H., **2021**. Uncovering Recent Progress in Nanostructured Light-Emitters for Information. *Light: Science & Applications*, 10, p.156. https://doi.org/10.1038/s41377-021-00598-3.

© Ariston Publications 2026. All rights reserved.

[29] Bahar, M. K. Başer, P., **2023**. The Second, Third Harmonic Generations Nonlinear Optical Rectification of the Mathieu Quantum Dot with the External. *Physica B: Condensed Matter*, 665, p.415042. https://doi.org/10.1016/j.physb.2023.415042.

[30] Ashrafi-Dalkhani, V. Ghajarpour-Nobegani, S. Karimi, M. J., **2019**. Effects of Spin-Orbit Interactions, External Fields Eccentricity on the Optical Absorption of an Elliptical Quantum Ring. *The European Physical Journal B*, 92, p.1-6. https://doi.org/10.1140/epjb/e2018-90691-5.

[31] Srivastav, R. K. Panwar, A., **2022**. Excitation of Terahertz Surface Magnetoplasmons by Nonlinear Mixing of Two Lasers on a Rippled Surface of Magnetized n-InSb. *Optik*, 264, p.169363. https://doi.org/10.1016/j.ijleo.2022.169363.

[32] Baskoutas, S. Paspalakis, E. Terzis, A. F., **2007**. Electronic Structure Nonlinear Optical Rectification in a Quantum Dot: Effects of Impurities External Electric Field. *Journal of Physics: Condensed Matter*, 19, p.395024. https://doi.org/10.1088/0953-8984/19/39/395024.

[33] Baskoutas, S. Paspalakis, E. Terzis, A. F., **2006**. Effects of Excitons in Nonlinear Optical Rectification in Semiparabolic Quantum Dots. *Physical Review B*, 74, p.153306. https://doi.org/10.1103/PhysRevB.74.153306.

[34] Karimi, M. J. Rezaei, G., **2011**. Effects of External Electric Magnetic Fields on the Linear Nonlinear Intersubb Optical Properties of Finite Semi-Parabolic Quantum Dots. *Physica B: Condensed Matter*, 406, p.4423-4428. https://doi.org/10.1016/j.physb.2011.08.105.

[35] Sakiroglu, S. Ungan, F. Yesilgul, U. Mora-Ramos, M. E. Duque, C. A. Kasapoglu, E. Sari, H. Sökmen, I., **2012**. Nonlinear Optical Rectification the Second Third Harmonic Generation in Pöschl-Teller Quantum Well under the Intense Laser Field. *Physics Letters A*, 376, p.1875-1880. https://doi.org/10.1016/j.physleta.2012.04.028.

[36] Karabulut, I. Şafak, H., **2005**. Nonlinear Optical Rectification in Semiparabolic Quantum Wells with an Applied Electric Field. *Physica B: Condensed Matter*, 368, p.82-87. https://doi.org/10.1016/j.physb.2005.06.040.

[37] Karabulut, I. Şafak, H. Tomak, M., **2005**. Nonlinear Optical Rectification in Asymmetrical Semiparabolic Quantum Wells. *Solid State Communications*, 135, p.735-738. https://doi.org/10.1016/j.ssc.2005.06.001.

[38] Hassanabadi, H. Liu, G. Lu, L., **2012**. Nonlinear Optical Rectification the Second-Harmonic Generation in Semi-Parabolic Semi-Inverse Quantum Wells. *Solid State Communications*, 152, p.1761-1766. https://doi.org/10.1016/j.ssc.2012.05.023.

[39] Jiang, Y. Q. Xu, J. H. Wang, W. J. Lu, X. Z. Liu, X. Wang, G. M. Li, F. M., **2001**. Second-Harmonic Generation Investigations of Asymmetric Coupled Quantum Wells. *Physical Review B*, 63, p.125308. https://doi.org/10.1103/PhysRevB.63.125308.

[40] Sedrakian, D. M. Khachatrian, A. Z. resyan, G. M. Badalyan, V. D., **2004**. The Second Harmonic Generation in the Symmetric Well Containing a Rectangular Barrier. *Optical Quantum Electronics*, 36, p.893-904. https://doi.org/10.1007/s11082-004-9606-4.

[41] Li, B. Guo, K.-X. Zhang, C.-J. Zheng, Y.-B., **2007**. The Second Harmonic Generation in Parabolic Quantum Dots in the Presence of Electric Magnetic Fields. *Physics Letters A*, 367, p.493-497. https://doi.org/10.1016/j.physleta.2007.03.046.

[42] Zhang, L. Xie, H.-J., **2003**. Electric Field Effect on the Second-Order Nonlinear Optical Properties of Parabolic Semiparabolic Quantum Wells. *Physical Review B*, 68, p.235315. https://doi.org/10.1103/PhysRevB.68.235315.

[43] Khordad, R. Ghanbari, A. Abbasi, K. Ghafaripour, A., **2023**. Harmonic Generation of Tuned Quantum Dots Including Impurity Effects. *Journal of Computational Electronics*, 22, p.260-265. https://doi.org/10.1007/s10825-022-01985-8.

[44] Ganeev, R. A. Kim, V. V. Shuklov, I. A. Popov, V. S. Lavrentyev, N. A. Ponomarenko, V. P. Mardini, A. A. Dyomkin, D. V. Milenkovic, T. Bundulis, A. Grube, J. Sarakovskis, A., **2022**. Third Harmonic Generation in the Thin Films Containing Quantum Dots Exfoliated Nanoparticles. *Applied Physics B*, 128, p.202. https://doi.org/10.1007/s00340-022-07923-7.

 © Ariston Publications 2026. All rights reserved.

[45] Duque, C. M. Mora-Ramos, M. E. Duque, C. A., **2013**. Properties of the Second Third Harmonics Generation in a Quantum Disc with Inverse Square Potential. A Modeling for Nonlinear Optical Responses of a Quantum Ring. *Journal of Luminescence*, 138, p.53-60. https://doi.org/10.1016/j.jlumin.2013.01.032.

[46] Zhang, L. Xie, H.-J., **2004**. Bound States Third-Harmonic Generation in a Semi-Parabolic Quantum Well with an Applied Electric Field. *Physica E: Low-Dimensional Systems Nanostructures*, 22, p.791-796. https://doi.org/10.1016/j.physe.2003.08.001.

[47] Wang, G., **2005**. Third-Harmonic Generation in Cylindrical Parabolic Quantum Wires with an Applied Electric Field. *Physical Review B*, 72, p.155329. https://doi.org/10.1103/PhysRevB.72.155329.

[48] Wang, G. Guo, K.-X., **2001**. Excitonic Effects on the Third-Harmonic Generation in Parabolic Quantum Dots. *Journal of Physics: Condensed Matter*, 13, p.8197-8206. https://doi.org/10.1088/0953-8984/13/35/324.

[49] Yu, Y. B. Wang, H. J., **2011**. Third-Harmonic Generation in Two-Dimensional Pseudo-Dot System with an Applied Magnetic Field. *Superlattices Microstructures*, 50, p.252-260. https://doi.org/10.1016/j.spmi.2011.07.001.

[50] Shao, S. Guo, K.-X. Zhang, Z.-H. Li, N. Peng, C., **2011**. Third-Harmonic Generation in Cylindrical Quantum Dots in a Static Magnetic Field. *Solid State Communications*, 151, p.289-292. https://doi.org/10.1016/j.ssc.2010.12.003.

[51] Shao, S. Guo, K.-X. Zhang, Z.-H. Li, N. Peng, C., **2010**. Studies on the Third-Harmonic Generations in Cylindrical Quantum Dots with an Applied Electric Field. *Superlattices Microstructures*, 48, p.541-549. https://doi.org/10.1016/j.spmi.2010.09.010.

[52] Zhai, W. Hassanbadi, H. Lu, L. Liu, G., **2014**. A Theoretical Study of Third-Harmonic Generation in Semi-Parabolic Plus Semi-Inverse Squared Quantum Wells. *Optics Communications*, 319, p.95-99. https://doi.org/10.1016/j.optcom.2013.12.075.

[53] Lis, K. Bednarek, S. Szafran, B. Adamowski, J., **2003**. Electrostatic Quantum Dots with Designed Shape of Confinement Potential. *Physica E: Low-Dimensional Systems Nanostructures*, 17, p.494-497. https://doi.org/10.1016/S1386-9477(02)00852-4.

[54] Yang, L. Xie, W., **2012**. Photoionization Cross Section of a Donor Impurity in a Two-Dimensional Anisotropic Quantum Dot. *Physica B: Condensed Matter*, 407, p.3884-3887. https://doi.org/10.1016/j.physb.2012.06.015.

[55] Fock, V., **1928**. Bemerkung zur Quantelung des Harmonischen Oszillators im Magnetfeld. *Zeitschrift für Physik*, 47, p.446-448. https://doi.org/10.1007/BF01390750.

[56] Darwin, C. G., **1931**. The Diamagnetism of the Free Electron. *Mathematical Proceedings of the Cambridge Philosophical Society*, 27, p.86-90. https://doi.org/10.1017/S0305004100009373.

[57] Halonen, V. Hyvönen, P. Pietiläinen, P. Chakraborty, T., **1996**. Effects of Scattering Centers on the Energy Spectrum of a Quantum Dot. *Physical Review B*, 53, p.6971-6974. https://doi.org/10.1103/PhysRevB.53.6971.

[58] Halonen, V. Pietiläinen, P. Chakraborty, T., **1996**. Optical-Absorption Spectra of Quantum Dots Rings with a Repulsive Scattering Centre. *Europhysics Letters*, 33, p.337-382. https://doi.org/10.1209/epl/i1996-00350-5.

© Ariston Publications 2026. All rights reserved.